Evaluation of Chemotherapy Response in VX2 Rabbit Lung Cancer with ^{18}F-Labeled C2A Domain of Synaptotagmin I

Feng Wang*[1,2], Wei Fang*[3,4], Ming-Rong Zhang[5], Ming Zhao[6], Biao Liu[7], Zizheng Wang[1], Zichun Hua[2], Min Yang[4], Katsushi Kumata[5], Akiko Hatori[5], Tomoteru Yamasaki[5], Kazuhiko Yanamoto[5], and Kazutoshi Suzuki[5]

[1]*Nanjing First Hospital, Nanjing Medical University, Nanjing, China;* [2]*State Key Laboratory of Pharmaceutical Biotechnology, Nanjing University, Nanjing, China;* [3]*Cardiovascular Institute and Fu Wai Hospital, Beijing, China;* [4]*Key Laboratory of Nuclear Medicine, Jiangsu Institute of Nuclear Medicine, Wuxi, China;* [5]*Molecular Imaging Center, National Institute of Radiological Science, Chiba, Japan;* [6]*Medical College of Wisconsin, Milwaukee, Wisconsin; and* [7]*Division of PET Centre, No. 1 Hospital, Nanjing Medical University, Nanjing, China*

The C2A domain of synaptotagmin I can target apoptotic cells by binding to exposed anionic phospholipids. The goal of this study was to synthesize and develop ^{18}F-labeled C2A-glutathione-*S*-transferase (GST) as a molecular imaging probe for the detection of apoptosis and to assess the response of paclitaxel chemotherapy in VX2 rabbit lung cancer. **Methods:** ^{18}F-C2A-GST was prepared by labeling C2A-GST with *N*-succinimidyl 4-^{18}F-fluorobenzoate (^{18}F-SFB). ^{18}F-C2A-GST was confirmed by high-performance liquid chromatography and sodium dodecyl sulfate polyacrylamide gel electrophoresis. The binding of ^{18}F-C2A-GST toward apoptosis was validated in vitro using camptothecin-induced Jurkat cells. Biodistribution of ^{18}F-C2A-GST was determined in mice by a dissection method and small-animal PET. Single-dose paclitaxel was used to induce apoptosis in rabbits bearing VX2 tumors (n = 6), and 2 VX2 rabbits without treatment served as control. ^{18}F-C2A-GST PET was performed before and at 72 h after therapy, and ^{18}F-FDG PET/CT was also performed before treatment. To confirm the presence of apoptosis, tumor tissue was analyzed and activated caspase-3 was measured. **Results:** ^{18}F-C2A-GST was obtained with more than 95% radiochemical purity and was stable for 4 h after formulation. ^{18}F-C2A-GST bound apoptotic cells specifically. Biodistribution in mice showed that ^{18}F-C2A-GST mainly excreted from the kidneys and rapidly cleared from blood and nonspecific organs. High focal uptake of ^{18}F-C2A-GST in the tumor area was determined after therapy, whereas no significant uptake before therapy was found in the tumor with ^{18}F-FDG–avid foci. The maximum standardized uptake value after therapy was 0.47 ± 0.28, significantly higher than that in the control (0.009 ± 0.001; $P < 0.001$). The apoptotic index was 79.81% ± 8.73% in the therapy group, significantly higher than that in the control (5.03% ± 0.81%; $P < 0.001$). Activated caspase-3 after paclitaxel treatment increased to 69.55% ± 16.27% and was significantly higher than that in the control (12.26% ± 5.39%; $P < 0.001$). **Conclusion:** ^{18}F-C2A-GST was easily synthesized by conjugation with ^{18}F-SFB and manifested a favorable biodistribution. Our results demonstrated the feasibility of ^{18}F-C2A-GST for the early detection of apoptosis after chemotherapy in a VX2 lung cancer model that could imitate the human lung cancer initiation, development, and progress.

Key Words: C2A domain; ^{18}F-labeled C2A-GST; PET; apoptosis; synaptotagmin I

J Nucl Med 2011; 52:592–599
DOI: 10.2967/jnumed.110.081588

Although the progression of cancer is a leading cause of death, oncologic medicine is adapting its strategy regarding cancer therapy and contributing to a personalized medicine approach. Because of its ability to measure therapeutic efficacy in vivo rapidly, molecular imaging has received growing attention and has shed light onto new avenues for assessing the therapeutic effect and determining the progression of disease (*1,2*). Successful chemotherapy or radiotherapy induces apoptosis in neoplastic cells, which can be a predictive indicator of a good therapy outcome in oncology (*3,4*). An early hallmark of apoptosis is the externalization of anion phospholipids including phosphatidylserine and phosphatidylinositide (*5,6*). Noninvasive imaging of cell death has been successfully applied in tumor models and clinical trials to determine whether apoptosis imaging could be a surrogate marker for monitoring therapeutic efficacy (*7–12*).

C2A domain of synaptotagmin I is an approximate 120–amino-acid segment with a common fold, an 8-strand antiparallel β sandwich connected by variable loops. In many C2 domains, binding of 2 or 3 Ca^{2+} ions in the 3 variable loops creates a substantial electrostatic potential that accelerates a protein's association. The C2A domain also binds anionic phospholipids with relatively high affinity (*13*). Our previous studies demonstrated that the technetium-labeled C2A-based molecular imaging probe ^{99m}Tc-C2A could target apoptotic cells not only in acute myocardial infarction but also in a tumor model (*14–18*). However, the biodistribution of ^{99m}Tc-C2A-glutathione-*S*-transferase (GST) is not optimal, and its main drawback is high uptake of radio-

Received Jul. 27, 2010; revision accepted Dec. 8, 2010.
For correspondence or reprints contact: Ming-Rong Zhang, Department of Molecular Probes, Molecular Imaging Center, National Institute of Radiological Science, 4-9-1 Anagawa, Inage-Ku, Chiba 263-8555, Japan.
E-mail: zhang@nirs.go.jp
*Contributed equally to this work.

activity in the kidneys and abdomen, severely hampering its clinical application, especially for imaging of abdominal tumors. It has been reported that ^{18}F-annexin V showed favorable characteristics of biodistribution and kinetics, compared with ^{99m}Tc-annexin V derivatives (*19–21*). Meanwhile, PET with higher spatial resolution and easily quantified calculation of standardized uptake value (SUV) may have more advantages in detecting apoptotic cells than other modalities including SPECT.

The current study aimed to synthesize and develop ^{18}F-labeled C2A-GST as a molecular imaging probe for detecting apoptosis and to assess the feasibility of early evaluation of paclitaxel chemotherapy outcome in a rabbit VX2 lung cancer model.

MATERIALS AND METHODS

General

^{18}F was produced by the ^{18}O (p,n) ^{18}F nuclear reaction using a Cypris HM-18 cyclotron (Sumitomo Heavy Industry). ^{18}F-FDG was provided by Andeco Co. If not otherwise stated, radioactivity was determined with an IGC-3R Curiemeter (Aloka). High-performance liquid chromatography (HPLC) was performed using an HPLC system (Jasco), and effluent radioactivity was monitored using an NaI(Tl) scintillation detector system. Ethyl 4-trimethylammoniumbenzoate triflate was synthesized as described previously (*22*). If not indicated, all chemical reagents were purchased from Sigma-Aldrich or Wako Pure Chem Industries and were of the highest grade commercially available. All procedures involving animals were performed in accordance with an institutional guideline (*23*) and the recommendations of the Committee for the Care and Use of Laboratory Animals, National Institute of Radiologic Sciences.

Expression and Purification of C2A-GST

A fusion protein C2A-GST of C2A and GST was overexpressed in *Escherichia coli* and purified as described previously (*24*).

Synthesis of *N*-Succinimidyl 4-^{18}F-Fluorobenzoate (^{18}F-SFB)

^{18}F-F^- was produced by the ^{18}O (p,n) ^{18}F reaction on 95% enriched ^{18}O-H_2O using 18-MeV protons (14.2 MeV on target) from the cyclotron. The ^{18}F-F^- in aqueous K_2CO_3 (3.3 mg/0.3 mL) was transported into a vial containing CH_3CN (1.5 mL)/Kryptofix 222 (15 mg; Merck) in a hot cell. The ^{18}F-F^- was dried to remove H_2O and CH_3CN at 110°C for 15 min. The residue was dissolved in 0.5 mL of anhydrous CH_3CN and concentrated under a nitrogen stream twice more. To the radioactive residue was added a solution of 10 mg of ethyl 4-(trimethylammonium triflate) benzoate in 0.2 mL of anhydrous dimethyl sulfoxide. The reaction mixture was sealed and heated at 110°C for 15 min. The hydrolysis step was performed by adding 0.5 mL of 1 M NaOH, followed by heating at 95°C for 10 min. After being cooled for 2 min, 0.8 mL of 1 M HCl was added to neutralize the reaction mixture. The mixture was then diluted to a final volume of 15 mL with distilled water and loaded onto a Waters Sep-Pak cartridge that was activated by passing 30 mL of CH_3CN and 30 mL of distilled water in advance through the device. The loaded cartridge was washed with 2 mL of 0.01 M HCl and blown dry for 2 min with a nitrogen stream. The radioactive fraction containing 4-^{18}F-flurobenzoic acid was eluted with 1.5 mL of CH_3CN.

The above radioactive fraction was treated with 20 μL of a 10% aqueous $(CH_3)_4NOH$ solution. The reaction mixture was dried in a nitrogen stream at 90°C, followed by the addition and evaporation of 1.5 mL of anhydrous CH_3CN. A solution of *O*-(*N*-succinimidyl)-*N,N,N′,N′*-tetramethyluronium tetrafluoroborate (15 mg) in 1 mL of CH_3CN was added, and the reaction mixture was heated at 90°C for 5 min. The mixture was concentrated to about 0.2 mL, cooled, and diluted with 0.2 mL of 5% aqueous acetic acid. HPLC semipreparative purification for this mixture was completed on a YMC J'Sphere ODS-H80 column (10-mm internal diameter × 250 mm) using a mobile phase of CH_3CN/H_2O (60/40) at a flow rate of 4.0 mL/min. The retention time for ^{18}F-SFB was 10.5 min. The fraction of ^{18}F-SFB was collected, diluted with 10 mL of distilled water, and loaded onto a Sep-Pak cartridge. The cartridge was blown dry with nitrogen and eluted with 2.5 mL of CH_3CN. The CH_3CN solution of ^{18}F-SFB was flowed into a 2-mL tube and evaporated to dryness under a gentle nitrogen stream at room temperature.

Synthesis of ^{18}F-C2A-GST

To the radioactive residue in the tube was added 0.2 mL of 0.1 M borate buffer (pH 8.4). This ^{18}F-SFB solution was added to a solution of 200 μg of C2A-GST in 50 μL of 0.2 M borate buffer (pH 8.4), and this mixture was maintained at room temperature for 20 min. The reaction mixture was purified by size-exclusion column chromatography with Bio-Gel P-6 (Bio-Rad).

Radiochemical Purity (RCP) Determination

HPLC. RCP was assayed by analytic HPLC (column: Bio-Rad HPLC Gel Filtration, Bio-Sil EC-125, 7.8-mm internal diameter × 300 mm; mobile phase: 0.05 M NaH_2PO_4/0.05 M Na_2HPO_4/0.2 M NaCl = 1/1/1). The retention time for ^{18}F-C2A-GST was 6.1 min at a flow rate of 1.0 mL/min.

Sodium Dodecyl Sulfate Polyacrylamide Gel Electrophoresis (SDS-PAGE). SDS-PAGE was performed with a Mini-Protein and PowerPac 300 (Bio-Rad). Laemmli sample buffer (Bio-Rad) was added to each sample (1:1) and applied to Ready-Gels J (Bio-Rad). Precision Protein Standard (Bio-Rad) was used as a standard. Electrophoresis was performed under constant voltage (200 V). After electrophoresis, gels were exposed to an imaging plate and radioactivity was analyzed by a BAS imaging system (BAS5000; Fujifilm), followed by staining with Bio-Safe Coomassie (Bio-Rad).

In Vitro Binding Assays

Apoptosis was induced in Jurkat cells (Riken Cell Bank) at a density of 5×10^6 cells/mL with 3.5 M camptothecin for 4 and 6 h (*15*). About 74 kBq of ^{18}F-C2A-GST were incubated with a 500-μL solution (pH 7.4) containing apoptotic or untreated cells (5×10^5), 15 mM *N*-(2-hydroxythyl) piperazine-*N*-9-(2-ethanesulfonic acid), 120 mM NaCl, and 2 mM $CaCl_2$. To separate cell-bound from free ^{18}F-C2A-GST, the mixture was centrifuged at 1,000 rpm for 2 min. After the aqueous supernatant was removed, the left radioactivity was measured.

Biodistribution Study in Mice

Male ddY mice (20–30 g; age, 7 wk; Japan SLC) were used. Each mouse was injected with ^{18}F-C2A-GST (~0.37 MBq/200 μL) via the tail vein. Three mice were sacrificed at 15, 60, and 120 min after injection by cervical dislocation. Whole-brain, liver, heart, lung, stomach, kidney, spleen, small intestine, and blood samples were quickly removed and weighed carefully. The radioactivity present in these tissues was measured using a

1480 Wizard γ-counter (Perkin-Elmer) and expressed as a percentage of the injected dose per gram of wet tissue. All radioactivity measurements were corrected for decay.

In Vivo Imaging with Small-Animal PET

PET scans were obtained using a small-animal PET Inveon scanner (Siemens Medical Solutions USA). Before the scans, mice were anesthetized with 1.5% (v/v) isoflurane and positioned on the scanner bed. After transmission scans for attenuation correction were acquired for 2 cycles (803 s) using a ^{57}Co point source, dynamic emission scans were acquired for 120 min in 3-dimensional list mode, with an energy window of 350–650 keV, immediately after intravenous injection of 1.85 MBq of ^{18}F-C2A-GST. All list-mode data were sorted into 3-dimensional sinograms, which were then Fourier-rebinned into 2-dimensional sinograms (frames, 4 × 1, 8 × 2, and 20 × 5 min). Dynamic images were reconstructed with filtered backprojection using a ramp filter. For data analysis, regions of interest were drawn on the lungs, heart, liver, and kidneys using ASIPro VM (Analysis Tools and System Setup/Diagnostics Tool; Siemens Medical Solutions USA), and the SUVs were acquired automatically. The maximum SUV (SUV_{max}) was calculated by measuring the maximal concentration of radioactivity in a region of interest and correcting it for body weight and injected dose (SUV_{max} = maximum activity concentration/[injected dose/body weight]). The time–radioactivity curves of different regions of interest were drawn. After the imaging experiments, the mice were sacrificed and tissues were removed for radioactivity measurement.

Metabolite Assay

After intravenous injection of ^{18}F-C2A-GST (1.85 MBq/200 μL) into ddy mice (n = 3), the mice were sacrificed by cervical dislocation at 15, 60, and 120 min, respectively. Blood samples were removed immediately and centrifuged at 15,000 rpm for 2 min at 4° C to separate plasma. Plasma (50 μL) was analyzed by HPLC under the same conditions described for the RCP determination. The ratio of unchanged ^{18}F-C2A-GST to total radioactivity on the HPLC chromatogram was calculated and expressed as a percentage.

VX2 Tumor Model in Rabbit Lung

Eight New Zealand White rabbits weighing 2–3 kg (Nanjing Medical University) were used in these experiments. The VX2 tumor is the biggest tumor model, which closely resembles human cancer. VX2 cells were initially grown in the hind limb of a donor rabbit. Each rabbit received general anesthesia with 3% pentobarbital (30 mg/kg) through an indwelling catheter in the auricular vein. The VX2 tumor was surgically removed from a donor rabbit under general anesthesia and minced into 1-mm^3 pieces with a pair of scissors. After the mouse received anesthesia, two 1.0-cm-deep tunnels were made bilaterally into the skin of the front chest, and one or two 1-mm^3 pieces of VX2 tissue were implanted into each tunnel. The incisions were closed with 3-0 sutures. When tumors had grown to approximately 10–20 mm in diameter, the rabbits were used in the experiment. Six rabbits bearing VX2 tumors received a single dose of paclitaxel treatment; 2 rabbits bearing tumors without treatment served as the control.

^{18}F-FDG PET/CT and Interpretation in VX2 Rabbit Tumor Model

^{18}F-FDG PET was performed in all rabbits bearing VX2 tumors in the right lung, which was fastened at least 6 h before scanning. ^{18}F-FDG (37 MBq) was injected into the rabbit via the auricular vein, and PET/CT was performed at 1 h after injection with a Gemini scanner (Philips Medical Systems). Emission data were acquired at 3 min per bed position; the CT component was performed using a multidetector scanner before the emission component. The parameters included 140 kV, 80 mA, 0.8 s per CT rotation, a pitch of 5.0 mm, and a table speed of 22.5 mm/s. Images were analyzed visually by 3 experienced nuclear medicine physicians. Interpretation was based on attenuation-corrected images. Any focal activity in a known lesion with an intensity higher than the normal mediastinal activity was considered malignant. Three experienced nuclear medicine physicians independently measured SUVs.

^{18}F-C2A-GST Imaging and Interpretation

Six rabbits bearing VX2 tumors in the right lung were treated by intravenous injection of paclitaxel (Nanjing Shike Pharmaceuticals) at the dose of 175 mg/m^2. Before and at 72 h after treatment, 18.5–37 MBq of ^{18}F-C2A-GST were injected via the auricular vein; PET/CT was performed at 2 h after injection with same protocol as those for ^{18}F-FDG. Images were analyzed and SUV analysis was also performed.

Histology and In Vitro Assay of Apoptosis

The investigated rabbits were sacrificed, and tumor tissues were excised after the imaging experiments. Each tissue specimen was divided into halves; one half was used for the histology analysis and the other for measuring the level of caspase-3. Caspase inhibitor, DEVD-FMK (Tocris Bioscience), conjugated to fluorescein isothiocyanate was used as a marker for direct determination of activated caspase-3. Caspase-3 activity was determined by flow cytometry using a commercial kit (CaspGLOW; BioVision) according to the manufacturer's protocol. DNA fragmentation was analyzed by terminal deoxynucleotidytransferase mediated dUTP nick-end labeling (TUNEL) assay using a commercial kit (Maxin-Bio). In random fields, TUNEL-positive nuclei as a percentage of total nuclei were determined and used as the apoptotic index.

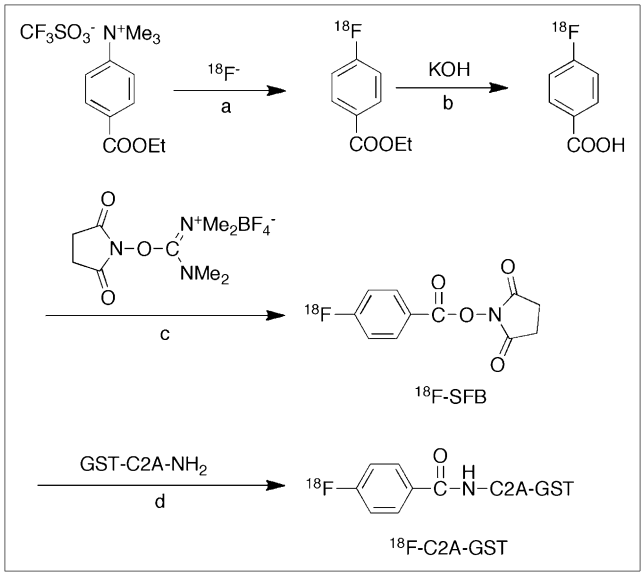

FIGURE 1. Synthesis scheme of ^{18}F-SFB and ^{18}F-C2A-GST. Reaction conditions include 110°C, CH_3CN, and 15 min (a); 95°C and 10 min (b); $(CH_3)_4NOH$, 90°C, CH_3CN, 5 min (c); and 0.1 M borate buffer (pH 8.4), room temperature, 20 min (d).

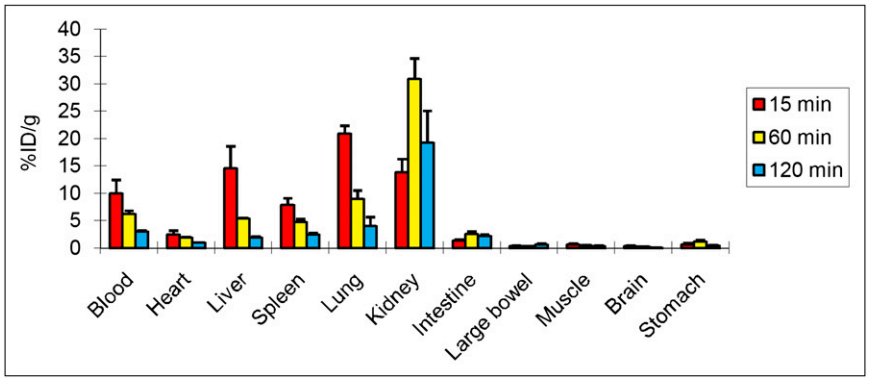

FIGURE 2. Biodistribution of ^{18}F-C2A-GST in mice at 15, 60, and 120 min after injection (n = 3 for each time point). Radioactivity was expressed as percentage of injected dose per gram of wet tissue (%ID/g).

Statistical Analysis

All data were expressed as mean ± SD. The statistical analysis was performed using SPSS 10.0 (SPSS Inc.), and paired t tests were used to show differences between 2 groups.

RESULTS

Synthesis of ^{18}F-C2A-GST

The decay-corrected radiochemical yield of ^{18}F-C2A-GST was 35%–40%, based on ^{18}F-SFB (Fig. 1). The synthesis time was about 2 h from the end of bombardment. The conjugating reaction was performed at room temperature. To guarantee the conjugation efficiency, a borate buffer (0.2 M, pH 8.4) was needed, and the concentration of the used protein (200 μg) was as high as possible. At the end of synthesis, 30–160 MBq of ^{18}F-C2A-GST (n = 6) were obtained as an intravenously injectable solution. After purification, the RCP of ^{18}F-C2A-GST was higher than 98%. The RCP remained 95% after maintaining the formulated product for 4 h at room temperature.

^{18}F-C2A-GST was not decomposed by any degradation of protein during synthesis and formulation. The autoradiograph and Coomassie staining of polyacrylamide after electrophoresis further verified that ^{18}F-C2A-GST exhibited high RCP.

In Vitro Assay

The binding specificity of ^{18}F-C2A-GST was evaluated with camptothecin-treated Jurkat cells. After inducement, a large number of apoptotic cells were observed at 4 h. After incubation with ^{18}F-C2A-GST, the uptake of radioactivity in the induced cells was 4.45 ± 0.6 (n = 4)-fold higher than that in the untreated cells ($P < 0.01$).

Biodistribution of ^{18}F-C2A-GST in Mice

The level of ^{18}F-C2A-GST uptake in organs is shown in Figure 2. The most predominant uptake of radioactivity was in the kidney, and the uptake decreased gradually with time. The uptake was significantly higher in the liver, spleen, and lungs at 15 min after injection and cleared rapidly with time, which reflected blood-pool activity. In contrast, uptake in the heart, gastrointestinal tract, and skeletal muscles was relatively lower. Rapid blood clearance was observed; the blood uptake was only 0.95 ± 0.09 percentage of the injected dose per gram of wet tissue at 120 min after injection.

Small-Animal PET Study

The images of ^{18}F-C2A-GST obtained by summing the uptake between 0 and 120 min after injection for the whole body of a normal mouse are shown in Figure 3B. Time–radioactivity curves in the main internal organs are shown in Figure 3A. The initial high uptake in the liver, lungs, and heart was visualized, and the radioactivity in the liver and

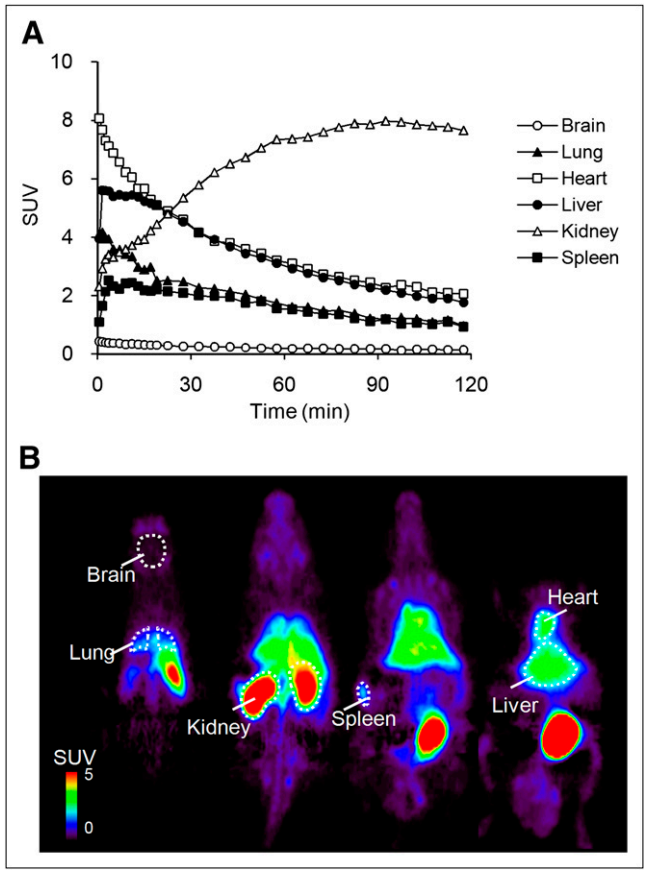

FIGURE 3. Small-animal PET of ^{18}F-C2A-GST in mice. (A) Time–radioactivity curves of ^{18}F-C2A-GST in main internal organs after PET dynamic acquisition. (B) Summation images of ^{18}F-C2A-GST between 0 and 120 min after radioligand injection.

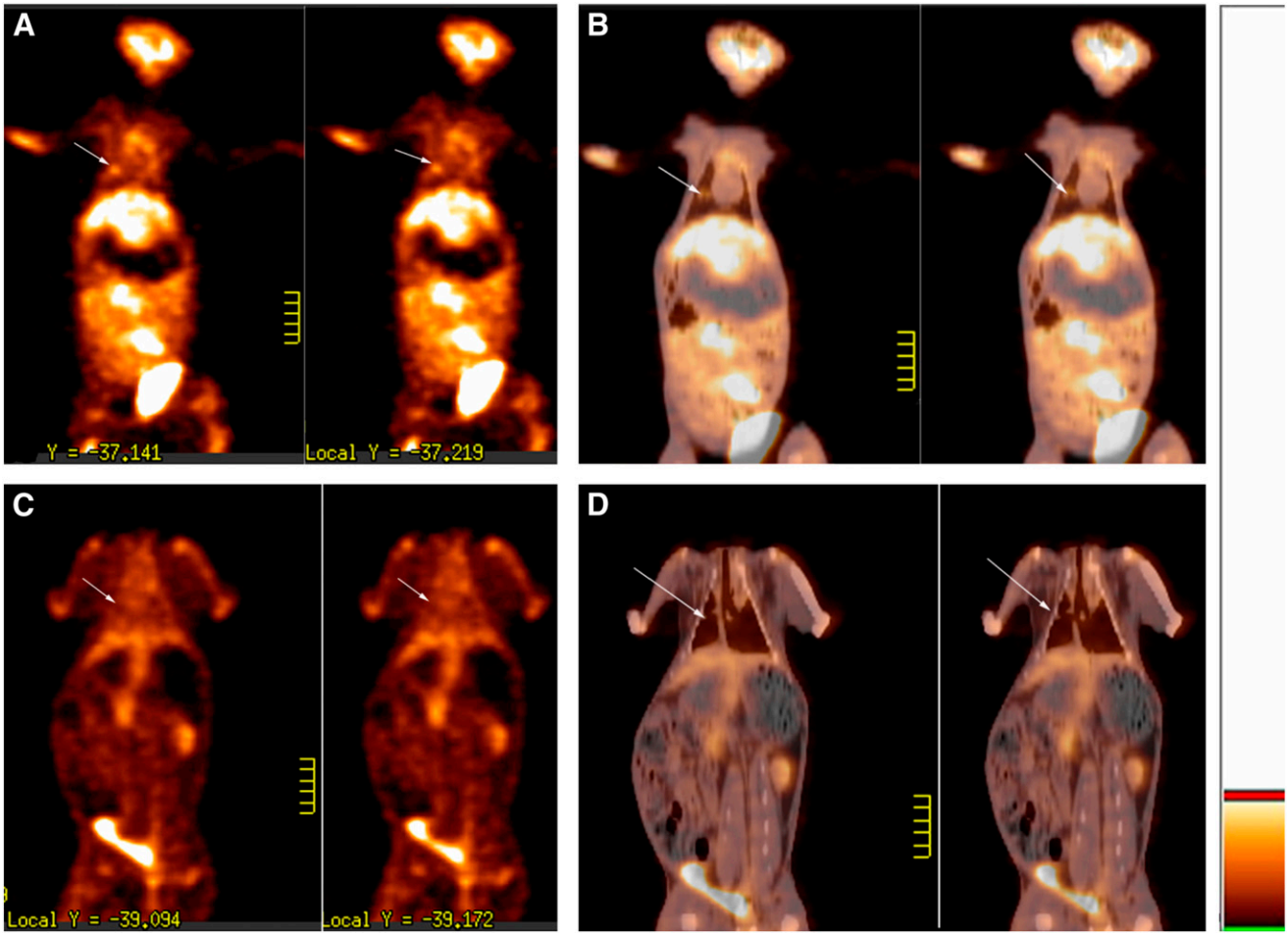

FIGURE 4. Neoplasm in right inferior lung in VX2 tumor model. Lesion was indicated by arrow. (A) ^{18}F-FDG PET images. ^{18}F-FDG–avid lesion was found in 2 sequential coronal sections. SUV_{max} was 1.9. (B) ^{18}F-FDG PET/CT fusion images. (C) ^{18}F-C2A-GST images. No significant accumulation of radioactivity was found in 2 sequential coronal sections before therapy. SUV_{max} was 0.01. (D) ^{18}F-C2A-GST PET/CT fusion images.

lungs peaked at 1.5 min after injection. The peak uptake in the heart was observed at 0.5 min and decreased slowly until the end of PET scanning. The radioactivity level in the kidneys increased gradually with time.

Metabolite Assay for Mouse Plasma

Metabolite analysis of ^{18}F-C2A-GST was performed for mouse plasma. ^{18}F-C2A-GST was stable, with about 90% unchanged form in the plasma at 120 min after injection.

^{18}F-FDG and ^{18}F-C2A-GST PET

Before therapy, focal uptake was visualized in primary tumor and lymph node adenopathy in ^{18}F-FDG images (Figs. 4A and 4B), whereas no significant uptake of ^{18}F-C2A-GST was found in the ^{18}F-FDG–avid foci (Figs. 4C and 4D)

After therapy by paclitaxel, intense uptake of ^{18}F-C2A-GST was found in the tumor area. Representative images are shown in Figure 5. By analyzing and comparing the images between therapy and nontherapy groups, the SUV_{max} of ^{18}F-C2A-GST after treatment was 0.47 ± 0.29 (n = 6), whereas that in the untreated group was 0.009 ± 0.001 (n = 2) ($P < 0.001$).

Tissue Analysis and Activated Caspase-3 Measurement

Representative results of the histologic analysis are shown in Figure 6. A small number of apoptotic cells were found before treatment (Figs. 6A and 6B)—characterized by cell shrinkage, condensed nuclei, and the appearance of apoptotic bodies. After the treatment, a large number of apoptotic cells were observed (Fig. 6C). The TUNEL-positive nuclei confirmed the DNA fragmentation (Fig. D). The apoptotic index was 79.81% ± 8.73% in the treated group, significantly higher than that in the untreated group (5.03% ± 0.81%; $P < 0.001$). Caspase-3 activity after paclitaxel therapy increased to 69.55% ± 16.27% and was significantly higher than that before therapy (12.26% ± 5.39%; $P < 0.001$).

DISCUSSION

Assessment of tumor shrinkage after therapy via anatomic imaging such as CT or MRI is still a gold standard in the evaluation of tumor response; however, such modalities often delay or do not adequately reflect the therapeutic efficacy, especially in targeted therapy (*25,26*).

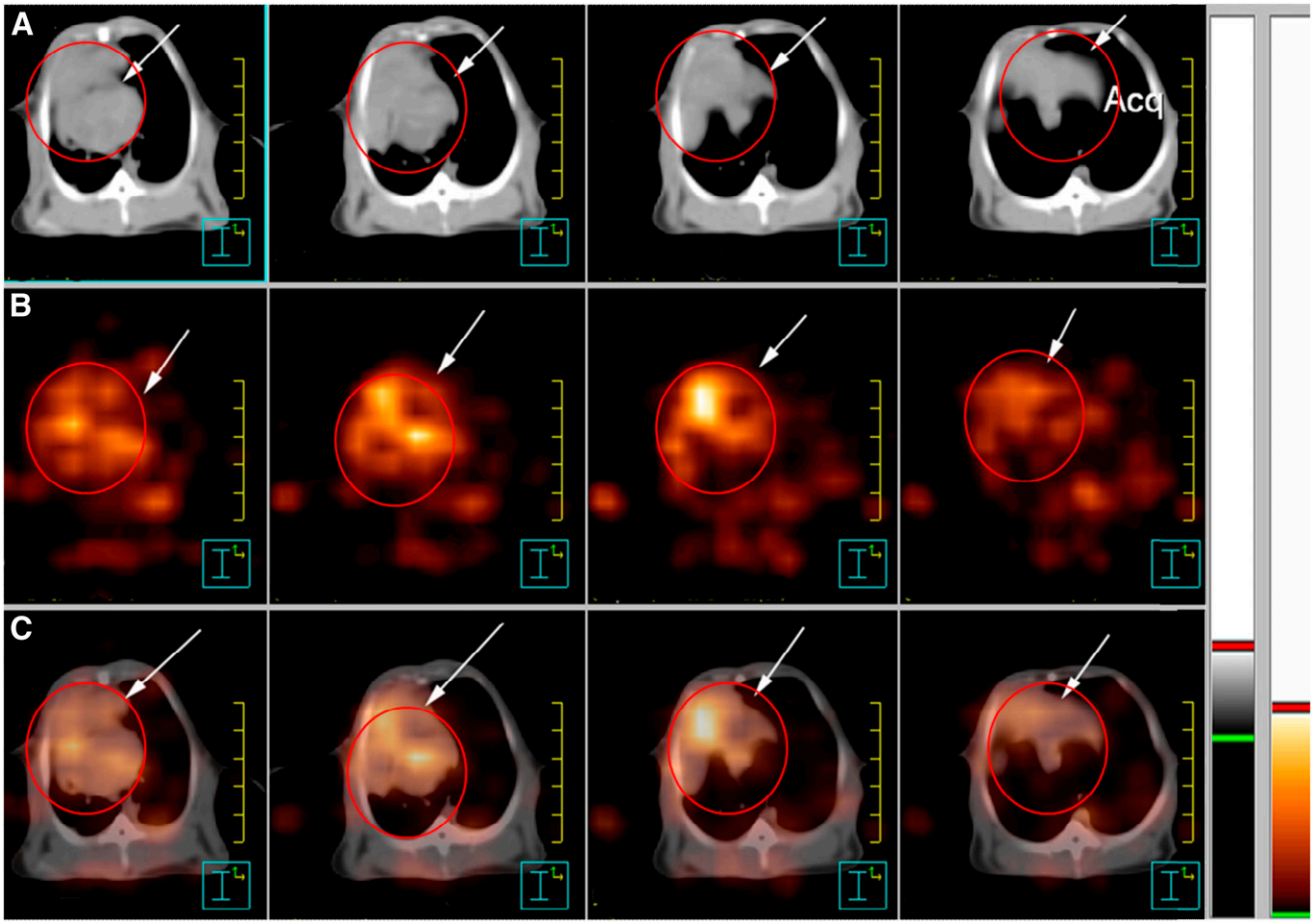

FIGURE 5. Large lesion at 72 h after paclitaxel therapy in anterior mediastinum and right lung in VX2 tumor model. Lesion is indicated by circle and arrow. (A) CT images of 4 sequential transverse sections. (B) ^{18}F-C2A-GST PET images. Intense uptake of radioactivity was found in tumor area. SUV_{max} was 0.75. (C) ^{18}F-C2A-GST PET/CT fusion images. Acq = acquisition.

Apoptosis is clearly one of the most fundamental biologic processes. Cumulative data have indicated that molecular imaging of apoptosis could be a useful tool in early evaluation of efficacy regarding cancer therapy (*8,9,27,28*). Moreover, attention is shifting toward personalized medicine, and local drug delivery through targeted therapy will likely increase the need for living molecular approaches to cell death imaging in the future.

In this study, we demonstrated the feasibility of ^{18}F-C2A-GST as a new potential radioligand for the detection of apoptosis and early evaluation of chemotherapy outcome by single-dose paclitaxel treatment in the VX2 lung cancer model using clinical PET/CT.

The C2A-GST fusion protein has been labeled with paramagnetic radionuclides such as ^{99m}Tc and used to detect apoptotic cells in vivo in our previous studies (*14–18*). Moreover, the latest study showed that ^{99m}Tc-C2A could be used in the early evaluation of chemotherapy in a mouse model bearing non–small cell lung cancer (*17*). However, a problem with C2A derivatives, including ^{99m}Tc-C2A, developed so far is that their biodistribution was not optimized and high nonspecific accumulation was observed in the abdominal organs. Moreover, the mouse tumor model could not really imitate human cancer initiation and development.

In this study, ^{18}F-C2A-GST was synthesized using ^{18}F-SFB as a labeling reagent with a reliable radiochemical yield. After radiolabeling, ^{18}F-C2A-GST could be purified efficiently and formulated without any degradation of protein. Moreover, this radioligand was stable for the time it took to acquire at least 2 PET scans (4 h).

Apoptosis is a dynamic process, and the most optimal window for the detection of apoptosis after chemotherapy is not known; in vivo stability of the radioligand in plasma is of great importance for the detection of apoptosis. As expected, the percentage of ^{18}F-C2A-GST was greater than 90% until 120 min after injection, thus confirming ^{18}F-C2A-GST as a favorable apoptosis-detecting imaging probe.

The biodistribution of ^{18}F-C2A-GST (Fig. 2) in normal mice showed ^{18}F-C2A-GST excreted mainly from the urinary tract. PET and time–radioactivity curves (Figs. 3A and 3B) in the mice further verified the favorable biodistribution profile, with rapid clearance from the blood and nonspecific organs. In this regard, the biodistribution profile of ^{18}F-C2A-GST, compared with that of ^{99m}Tc-C2A, may show some merits for detecting apoptosis and facilitating clinical application.

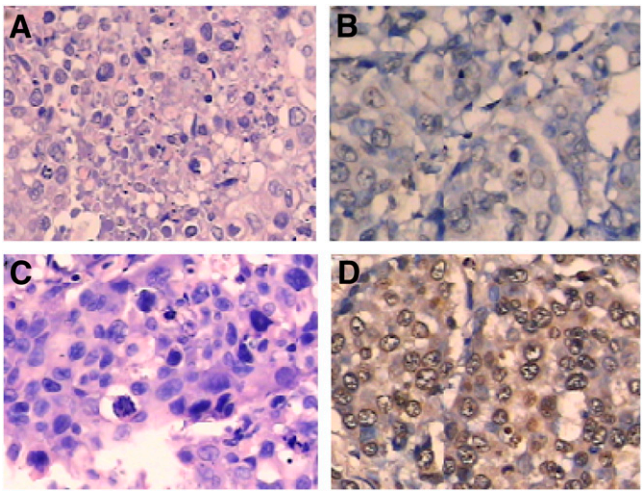

FIGURE 6. Histologic staining of tumor tissues before and after 72 h of chemotherapy. (A and B) Hematoxylin and eosin staining (A) and TUNEL staining (B) before therapy. (C and D) Corresponding staining after therapy.

Eight rabbits with VX2 lung cancer (squamous carcinoma) were used in this study. Three of the 8 rabbits bore lymph node adenopathy, 3 bore metastasis in the contralateral lung, and 2 bore pleural invasion, which was confirmed by PET/CT and by histopathology after sacrifice. To our knowledge, VX2 is the biggest tumor model of lung cancer, and can closely imitate human lung cancer initiation, development, and progress. Before therapy with paclitaxel, no significant accumulation of ^{18}F-C2A-GST was found in the tumor area with ^{18}F-FDG–avid foci (Fig. 4). High focal uptake of ^{18}F-C2A-GST was visualized in the tumor at 72 h after therapy (Fig. 5). The SUV_{max} of the tumor after treatment was significantly higher than that of the untreated tumor. A large number of TUNEL-positive nuclei were observed (Fig. 6). Hematoxylin and eosin staining further showed that a large number of apoptotic cells associated with cell shrinkage, condensed nuclei, and apoptotic bodies were found at 72 h after therapy, whereas only a small number of apoptotic cells were found in the control. Activated caspase-3 activity in the tumor area was significantly increased after therapy. This finding revealed that the increased accumulation of ^{18}F-C2A-GST in the tumor after paclitaxel therapy was caused by the ongoing apoptosis. These results indicate that it is feasible to detect apoptosis with ^{18}F-C2A-GST in a VX2 lung cancer model used to mimic human lung cancer. ^{18}F-C2A-GST may thus hold more prospects in translation from bench to clinic, especially in monitoring the efficacy of anticancer therapy.

The C2A domain is a compact 8-strand sheet structure interconnected by 7 loops. The Ca^{2+} and phosphatidylserine binding sites are formed by 3 loops at the top of this domain. There are 3 sites for Ca^{2+} in the Ca^{2+} binding pocket of C2A, and this binding stabilizes the loops while producing no significant conformational changes (*29,30*). The empty coordination sites on the bound Ca^{2+} ions are filled by direct interaction with anionic phospholipids. Despite the distinct structural differences between C2A and annexin V, C2A can be conjugated as efficiently with ^{18}F-SFB as can annexin V. Moreover, ^{18}F-C2A-GST was shown to have levels of in vitro and in vivo uptake similar to those of ^{18}F-annexin V in the same tumor cells and animals (data not shown). Therefore, ^{18}F-C2A-GST may serve as an alternative molecular imaging probe for the detection of cell death.

A limitation of this study is nonspecific accumulation of radioactivity in the intestines after therapy, which might be due to inflammation and injury caused by paclitaxel chemotherapy. Furthermore, because the limited number of controls prevented correlation analysis from being performed, ^{18}F-C2A-GST warrants further investigation in term of biodistribution on tumor-bearing animals before and after chemotherapy. However, this study may pave the way for the use of molecular imaging of apoptosis in the early evaluation of the efficacy of anticancer therapy.

CONCLUSION

^{18}F-C2A-GST was easily labeled by the conjugation of the fusion protein C2A-GST with ^{18}F-SFB. The in vitro and in vivo evaluation demonstrated the feasibility of ^{18}F-C2A-GST for the early detection of apoptosis after chemotherapy in a VX2 lung cancer model that could imitate human cancer development and progress. When radiolabeling is fully optimized and preclinical evaluation is finished, ^{18}F-C2A-GST may serve as a potential early surrogate marker for therapeutic efficacy in tumors.

ACKNOWLEDGMENTS

We thank to Nobuki Negaki (SHI Accelerator Service) for radiochemistry assistance. We also thank the staff of the National Institute of Radiological Sciences for support in the cyclotron operation, radioisotope production, and animal experiments. This study was financially supported in part by Nuclear Researchers Program 2007 from the Ministry of Education, Culture, Sports, Science and Technology of the Japan government, Jiangsu Government-Science (grant BS2006010), National Nature Science Foundation of China (grant 30700186 30500134), and key laboratory of Nuclear Medicine, Ministry of Health (KF200902), China.

REFERENCES

1. Blankenberg FG. In vivo detection of apoptosis. *J Nucl Med.* 2008;49(suppl 2):81S–95S.
2. Brindle K. New approaches for imaging tumour responses to treatment. *Nat Rev Cancer.* 2008;8:94–107.
3. Joseph B, Lewensohn R, Zhivotovsky B. Role of apoptosis in the response of lung carcinomas to anti-cancer treatment. *Ann N Y Acad Sci.* 2000;926: 204–216.
4. Amezcua CA, Lu JJ, Felix JC, et al. Apoptosis may be an early event of progestin therapy for endometrial hyperplasia. *Gynecol Oncol.* 2000;79:169–176.
5. Belhocine T, Steinmetz N, Hustinx R, et al. Increased uptake of the apoptosis-imaging agent ^{99m}Tc recombinant human Annexin V in human tumors after one course of chemotherapy as a predictor of tumor response and patient prognosis. *Clin Cancer Res.* 2002;8:2766–2774.

6. Williamson P, Schlegel RA. Transbilayer phospholipid movement and the clearance of apoptotic cells. *Biochim Biophys Acta.* 2002;1585:53–63.
7. Fadok VA, Voelker DR, Campbell PA, Cohen JJ, Bratton DL, Henson PM. Exposure of phosphatidylserine on the surface of apoptotic lymphocytes triggers specific recognition and removal by macrophages. *J Immunol.* 1992;148:2207–2216.
8. Kartachova M, van Zandwijk N, Burgers S, et al. Prognostic significance of ^{99m}Tc Hynic-rhannexin V scintigraphy during platinum-based chemotherapy in advanced lung cancer. *J Clin Oncol.* 2007;25:2534–2539.
9. Rottey S, Slegers G, Van Belle S, et al. Sequential ^{99m}Tc-hydrazinonicotinamide-annexin V imaging for predicting response to chemotherapy. *J Nucl Med.* 2006;47:1813–1818.
10. Tait JF, Smith C, Blankenberg FG. Structural requirements for in vivo detection of cell death with ^{99m}Tc-annexin V. *J Nucl Med.* 2005;46:807–815.
11. Petrovsky A, Schellenberger E, Josephson L, et al. Near-infrared fluorescent imaging of tumor apoptosis. *Cancer Res.* 2003;63:1936–1942.
12. Lahorte CMM, VanderHeyden JL, Steinmetz N, et al. Apoptosis-detecting radioligands: current state of the art and future perspectives. *Eur J Nucl Med Mol Imaging.* 2004;31:887–919.
13. Davletov BA, Sudhof TC. A single C2A domain from synaptotagmin I is sufficient for high affinity Ca2+/phospholipid binding. *J Biol Chem.* 1993;268: 26386–26390.
14. Zhao M, Beauregard DA, Loizou L, Brindle KM. Non-invasive detection of apoptosis using magnetic resonance imaging and a targeted contrast agent. *Nat Med.* 2001;7:1241–1244.
15. Zhao M, Zhu X, Ji S, et al. ^{99m}Tc labeled C2A domain of synaptotagmin I as a target-specific molecular probe for the non-invasive imaging of acute myocardial infarction. *J Nucl Med.* 2006;47:1367–1374.
16. Fang W, Wang F, Ji S, et al. SPECT imaging of myocardial infarction using ^{99m}Tc-labeled C2A domain of synaptotagmin I in a porcine ischemia–reperfusion model. *Nucl Med Biol.* 2007;34:917–923.
17. Wang F, Fang W, Zhang M, et al. Imaging Paclitaxel (chemotherapy) induced tumor apoptosis with ^{99m}Tc C2A a domain of synaptotagmin I: a preliminary study. *Nucl Med Biol.* 2008;35:359–364.
18. Liu Z, Zhao M, Zhu X, et al. In vivo dynamic imaging of myocardial cell death using ^{99m}Tc-labeled C2A domain of synaptotagmin I in a rat model of ischemia and reperfusion. *Nucl Med Biol.* 2007;34:907–915.
19. Zijlstra S, Gunawan J, Burchert W. Synthesis and evaluation of a ^{18}F-labelled recombinant annexin-V derivative, for identification and quantification of apoptotic cells with PET. *Appl Radiat Isot.* 2003;58:201–207.
20. Murakami Y, Takamatsu H, Taki J, et al. ^{18}F-Labeled annexin V: a PET tracer for apoptosis imaging. *Eur J Nucl Med Mol Imaging.* 2004;31:469–474.
21. Yagle KJ, Eary JF, Tait JF, et al. Evaluation of ^{18}F-annexin V as a PET imaging agent in an animal model of apoptosis. *J Nucl Med.* 2005;46:658–666.
22. Guhlke S, Coenen HH, Stocklin G. Fluoroacylation agents based on small n.c.a. [^{18}F]fluorocarboxylic acids. *Appl Radiat Isot.* 1994;45:715–727.
23. *Guide for the Care and Use of Laboratory Animals*. Washington, DC: National Academy Press; 1996.
24. Zhang X, Rizo J, Sudhof TC. Mechanism of phospholipid binding by the C2A-domain of synaptotagmin I. *Biochemistry.* 1998;37:12395–12403.
25. Ramnath N, Sommers E, Robinson L, et al. Phase II study of neoadjuvant chemotherapy with gemcitabine and vinorelbine in resectable non-small cell lung cancer. *Chest.* 2005;128:3467–3474.
26. Shepherd FA, Rodrigues Pereira J, Ciuleanu T, et al. Erlotinib in previously treated non-small-cell lung cancer. *N Engl J Med.* 2005;353:123–132.
27. Brown JM, Attardi LD. The role of apoptosis in cancer development and treatment response. *Nat Rev Cancer.* 2005;5:231–237.
28. Ntziachristos V, Schellenberger EA, Ripoll J, et al. Visualization of antitumor treatment by means of fluorescence molecular tomography with an AnnexinV-Cy5.5 conjugate. *Proc Natl Acad Sci USA.* 2004;101:12294–12299.
29. Sutton RB, Davletov BA, Berghuis AM, et al. Structure of the first C2 domain of synaptotagmin I: a novel Ca2+/phospholipid-binding fold. *Cell.* 1995;80:929–938.
30. Shao X, Fernandez I, Sudhof TC, et al. Solution structures of the Ca2+-free and Ca2+-bound C(2)A domain of synaptotagmin I: does Ca2+ induce a conformational change? *Biochemistry.* 1998;37:16106–16115.